Three-Dimensional Demarcation of Perfusion Zones Corresponding to Specific Coronary Arteries: Application for Automated Interpretation of Myocardial SPECT

Piotr J. Slomka, Gilbert A. Hurwitz, Grace St. Clement and Janice Stephenson

Department of Diagnostic Radiology and Nuclear Medicine, University of Western Ontario and Victoria Hospital, London, Ontario, Canada

In this study, three-dimensional maps of specific coronary artery territories were derived and combined with normal distribution maps as a reference for automated characterization of defects, including location and size. **Methods:** One hundred sixty-eight ^{99m}Tc-sestamibi myocardial perfusion SPECT scans from normal patients and patients with single-vessel disease were selected according to angiographic data. Five separate groups were established for men and women: normal, proximal left anterior descending (PLAD), distal left anterior descending (DLAD), right coronary artery (RCA) and left circumflex (LCx). All myocardial perfusion studies were aligned and sized to the same three-dimensional orientation using a previously developed automated image registration technique. Mean and variation three-dimensional templates were constructed from stress images in each group. Normal templates were demarcated with hypoperfusion regions obtained from disease templates. The defects were detected in the individual patient's images by a region-growing algorithm which identified abnormal voxels by comparison to the corresponding voxels in the mean and variation templates. **Results:** Defects were quantified with respect to volume, location relative to the expected hypoperfusion zones and severity index. Abnormal regions could be marked directly on tomographic slices and visualized in various orientations. Single defects greater than 2% of the myocardium positioned within demarcated perfusion territories were detected in 105/119 abnormal patients and in 3/49 normal patients. **Conclusion:** Maps of myocardial perfusion zones created from images of angiographically selected patients provide a reference for automated localization of myocardial perfusion defects. A template-based region-growing is a robust technique for volumetric quantification and localization of abnormal regions.

Key Words: myocardial perfusion tomography; quantification; automated analysis; perfusion zones

J Nucl Med 1995; 36:2120–2126

An important aspect of myocardial perfusion interpretation is the localization and sizing of diseased portions of the myocardium. Perfusion defect sites should correspond to anatomical locations of diseased arteries. Therefore, by analyzing defect location, it should be possible to optimally predict which of the three arteries are involved in coronary artery disease. Size and severity of the abnormal areas can be related to the extent of the hypoperfusion. Visual methods of assigning the defect to a given coronary artery are highly subjective because of differences in coronary artery anatomy and variations in defect size. Thus, an automated method for localizing defects could be a valuable step toward computer-aided interpretation of myocardial perfusion images.

Previously, we developed an algorithm for automated fitting of patient images to three-dimensional normal templates (*1*). This study seeks to demarcate the normal templates with gender-specific three-dimensional maps of myocardial perfusion territories corresponding to specific coronary arteries, which would allow automated assignment of defects to perfusion territories. The maps of defect territory along with normal templates effectively provide a three-dimensional reference atlas for automated interpretation of myocardial perfusion tomography. By fitting and comparing the test-patients' images to such a model, defects could be characterized objectively.

METHODS

Patient Selection

One hundred sixty-eight men and women with single-vessel disease and normal patients were selected from approximately 400 individuals who had correlated ^{99m}Tc-sestamibi studies of tomographic perfusion and angiography, which were accumulated over 2 yr. Studies were excluded if:

1. Coronary artery bypass surgery had previously been performed.
2. Either study (scan or angiogram) was performed within 1 wk of myocardial infarction.

Received Nov. 3, 1994; revision accepted May 15, 1995.

For correspondence or reprints contact: Piotr Slomka, PhD, Department of Nuclear Medicine, Victoria Hospital, 375 South St., London, Ontario, Canada N6A 4G5.

3. Angiographic or other data suggested another cause of the disease (rheumatic valvular disease or idiopathic cardiomyopathy, etc.).

If angioplasty had been previously performed, it was required that a period of 3 mo elapse before follow-up assessment and that angiography and imaging be performed within 3 mo of each other. If there had been no previous angioplasty, a 4-mo interval between imaging and angiography was allowed. The angiograms and scintigraphic studies were ordered based on the usual clinical indications and were interpreted and reported by standard clinical procedures.

All angiograms were interpreted by a single cardiovascular radiologist blinded to the scintigraphic results and rated as previously reported (*2*). Angiographically normal cases used for the construction of normal gender-specific templates met the following criteria: (a) no left mainstem stenosis greater than 30%, (b) no stenosis in the main arteries or branches greater or equal to 50% luminal diameter. Patients with a history of myocardial infarction but no significant stenoses were excluded if: (a) Q-waves were present or if (b) there was a history of a non-Q-wave infarction with an unequivocal resting scan defect, or abnormal contrast ventriculogram. Patients were designated as having single-vessel disease in the LAD, RCA or LCx sites if they met the following criteria: (a) no left mainstem lesion larger than 30%, (b) a lesion of 70% or greater in one of the three main arteries, (c) no lesions in other main arteries or branches of 50% or greater; for the LCx site only, because of the relative paucity of patients, a second site of up to 50% stenosis was allowed. Patients with LAD stenoses were further divided into those with proximal (PLAD) disease (before the first septal perforator artery) and those with more distal disease (DLAD).

Exercise and Image Acquisition and Reconstruction Protocols

Each patient underwent an individually-tailored stress protocol with intravenous dipyridamole, exercise or a combined procedure, as previously described (*3*). The injected dose was dependent on the patient's weight (0.32 mC/kg in the exercise study). Stress images were collected 1 hr postinjection. Images were acquired on a Siemens (Hoffman Estates, IL) ZLC 7500 NCO single-head camera with a low-energy, all-purpose collimator. Data were collected using 180° rotation, 64 × 64 matrix, 32 stops, 30 sec/stop and a circular orbit. The pixel size of the acquisition data was 6.3 mm. The data were reconstructed on a Nuclear Diagnostics (Stockholm, Sweden) HERMES workstation. Two-dimensional Metz adaptive prefiltering of projection frames was applied. Reconstruction by filtered backprojection was performed without applying attenuation correction.

In the majority of studies, most of the external activity was automatically eliminated by setting to zero voxels outside circular outlines (diameter equal to the matrix size) positioned perpendicular to the transverse slices. In 15 patients, significant areas of activity in the abdomen were not sufficiently removed by this procedure. These areas were masked from the reconstructed slices by interactively drawing regions of interests. The reconstruction and the masking operation were the only steps requiring user interaction. Rest images were not used in this study because the goal was to localize hypoperfusion zones.

Computer Processing Algorithms

All computer algorithms were implemented in the C programming language using the Solaris operating environment and a SUN SPARC 10/512 workstation.

Three-Dimensional Image Registration. Reconstructed transverse stress images were aligned to a common three-dimensional orientation and size by the automated algorithm previously developed in our laboratory (*1*). Briefly, the algorithm aligned and sized images three-dimensionally by independently adjusting nine transformation parameters (three scalings, three translations and three rotations). After the initial principal axes transformation (*4*), the algorithm performed downhill-simplex iterative minimization (*5*) of the sum of absolute count differences between the images of individual patients; each iteration involved a full reorientation of image volume (64 × 64 × 32 voxels). Thus, there was no need for manual definition of angles, position or edges of the myocardium during reconstruction.

Creating Mean and Variation Templates. The aligned images were used to create three-dimensional reference templates. A refined, two-stage approach was used to build the templates. In the first stage, patients were sequentially registered and cumulatively added voxel-by-voxel after normalization to the maximum count in the myocardium, as described previously (*1*). The male template built in this way was then resized to the mean scaling parameters in three directions (X, Y, Z); the mean scaling parameters were derived from the registration results of the male group. Therefore, the dimensions of the male template reflected the average dimensions in this group. The female mean template was resized to the male template dimensions, which allowed direct comparison of both groups.

In the second stage, original images of normal patients were re-registered to the resized templates. This time, all individual scans were registered to the same, previously accumulated templates. The individual studies were normalized using the reciprocal of the ratio of maximum-count (averaged in the 3 × 3 × 2 voxel region) in the patient's images and the count value at the corresponding location in the mean template derived in the first stage. A new template was then constructed by calculating the mean of normalized counts at each voxel. Thus, the construction of the templates during the second stage was independent of the order in which patients were registered; therefore, true mean voxel values were calculated. Subsequently, the three-dimensional variation templates were obtained by calculating the coefficient of variation (standard deviation divided by the mean) of the count distribution at each voxel.

Finally, all normal and abnormal patient datasets were registered to gender-specific templates created in the second stage. The process was fully automatic, and the same algorithm and parameters were applied to all test patients without any individual adjustments. An experienced nuclear medicine technologist visually assessed the quality of the automated fitting for each test patient, but manual adjustment of registration parameters was not permitted. Abnormal patient datasets were then used to build separate mean templates representing the disease in particular territories (PLAD, DLAD, RCA, LCx). Four male (PLAD, DLAD, RCA, LCx) and three female (LAD, RCA, LCx) disease templates were constructed. Disease templates were built in the same manner as the normal ones. Normal and disease templates were correlated to the same orientation and size, because all individual studies were registered to the same reference.

Template-Based Region-Growing Technique. To estimate the size and location of perfusion defects, a three-dimensional recursive

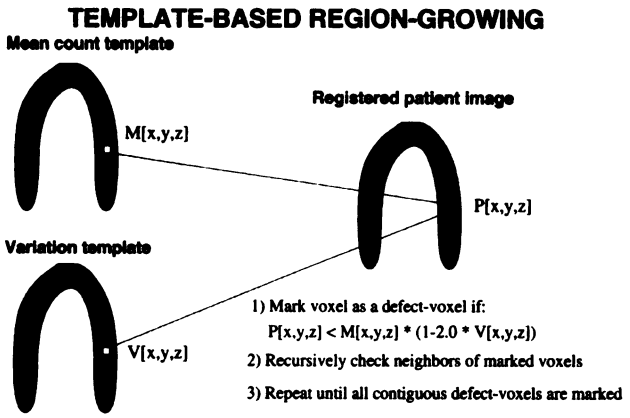

FIGURE 1. Template-based region growing technique. Voxels with values smaller than 2 s.d.s below the mean are marked as abnormal.

region-growing scheme was implemented, based on a two-dimensional version of the algorithm (*6*). The algorithm used the variation and mean templates to mark contiguous voxels in the patient image that were below normal limits (Fig. 1).

The counts in the test patient images were normalized using the reciprocal of the ratio of the maximum count (averaged in the 3 × 3 × 2 voxel region) and the count value at the corresponding location in the mean templates. The region-growing technique was initiated from the point at which the difference between voxel values of the test patient image and the mean template image divided by the coefficient of variation at that location was maximal. To reduce the effect of noise, this difference was evaluated in a 3 × 3 × 2 voxel region. The points in the three-dimensional neighbourhood of the initial point were then considered. The region-growing technique marked all contiguous voxels (belonging to one three-dimensional cluster) if their value was smaller than the mean minus a predefined s.d. threshold (Fig. 1), which was set to 2.0 s.d. for all test patients. It was assessed visually that a 2.0 s.d. threshold provided the outline of the region most consistent with visual interpretation compared to 1.5, 1.75, 2.25 and 2.5 s.d. thresholds. The region-growing procedure was repeated three times, avoiding the previously marked voxels. Therefore, it was possible to derive up to three separate defects on the patient data. This repetiton of the region-growing procedure was necessary to ensure that all defective areas were included. Although we analyzed only patients with single-vessel disease, the first detected region in 4 patients was a small spurious defect (usually on the edge) and the true defect was found after the algorithm was reapplied. During the third application of the region-growing algorithm, small defects were found in only 7 of 168 patients; none of them was related to the primary hypoperfusion site. Nevertheless, in most patients, only one region was found or the secondary regions were negligible in size (<1% of myocardium); thus, multiple regions were merged for further calculations.

Determining Perfusion Zones of Specific Coronary Arteries. To estimate the average perfusion zones in each angiographic group, the region-growing procedure was applied to the disease templates. Because the templates, accumulated from many patients, were smooth in appearance, the s.d. thresholds for the region-growing procedure were reduced. The threshold was individually adjusted for each of the disease templates. This was done to obtain the size of the coronary artery territory equal to the average size of the defects derived individually for each patient. The resulting disease regions were coded as three-dimensional bitmap images, allowing voxels to belong to more than one region (thus permitting overlap between territories). Separate three-dimensional maps of hypoperfusion zones were constructed for men and women. The DLAD territory was mostly included in the PLAD region; therefore, these two regions were merged for quantification purposes. Thus, three separate perfusion zones (LAD, LCx, RCA) were established for men and women.

Quantification of Defect Extent, Severity and Location. The template-based region-growing procedure was applied to each of the test patient images. The percentages of the defect belonging to each territory and to undesignated areas were calculated by counting the overlapping voxels belonging to the defect and a particular perfusion zone. Also, the percentage of each territory covered by the patient's defect was calculated. Several other quantitative parameters were derived for the abnormal regions. The derived parameters included the following: absolute (cm^3) and relative defect volumes (percentage of myocardial volume), defect severity (average number of s.d.s below the mean), centroid coordinates and severity product (a multiplication of severity and defect size). The absolute volume was calculated by dividing the volume of the resized defect by X, Y and Z scaling parameters. The severity product provided a measure of missing counts in the myocardium.

Defect Visualization. The display of the original tomographic images and defects was integrated by overlaying the bitmap images representing the abnormal voxels outlined by the region-growing algorithm on the original patient images. Patient data could also be displayed in the original dimensions (before the alignment to the template). For this purpose, inverted registration scaling parameters were used to resize the patient images and defect bitmaps.

RESULTS

The normal templates were similar in appearance to the templates created in the previous study (*1*). Tomographic slices of the male variation template are shown in Figure 2. An example of the region-growing and quantification results in a test-patient with the LCx defect is shown in Figure 3. The LCx, RCA and PLAD disease templates with superimposed defect territories in men are shown in Figures 4 and 5, respectively. The DLAD territory was mostly included in the PLAD region; therefore, for defects localization, these two regions were combined into one LAD territory.

The results of region-growing procedure are summarized in Table 1. Studies with defects ≥2% of myocardial volume were considered abnormal. The results in Table 1 are derived from stress scans only and include only well-defined cases (70% or greater stenoses). Therefore, they should not be treated as representing the sensitivity or specificity of the test but rather as a demonstration of region-growing quantification in individual patients. Defects were assigned to the perfusion zone containing the largest portion of the abnormal region. The defect was considered to be unassigned if more than 50% of defect voxels were located outside of the designated zones and it did not cover more than 10% of any of the designated perfusion zones (small spurious defects). These criteria were arbitrarily selected to

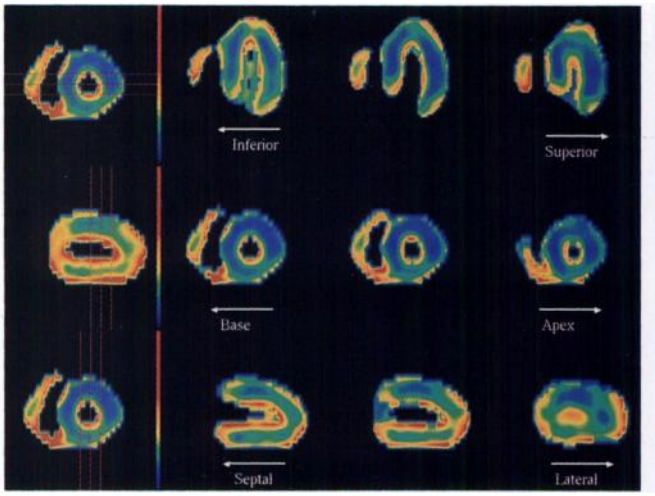

FIGURE 2. Horizontal long-axis (top), short-axis (middle) and vertical long-axis (bottom) of the variation template. Higher variation is observed on edges due to shape differences between images included in the template. The lowest values of the coefficient of variation (blue, 7%) are located in the high lateral regions; the highest values (red, 50%) are located on the edges. The voxels outside the mean template outline (defined as less than 15% of the maximum) are masked.

reflect visual interpretation of the scan by a clinician. To precisely determine the optimal values for defect classification, a prospective analysis of these parameters would have to be performed on a separate set of test patients representing a full clinical population.

Based on these criteria, defects were identified in 9 of 49 normal patients, but only 3 of these were in regions of the myocardium designated as perfusion zones. Only one of these patients was classified as normal based on visual analysis. A unique defect was identified in most of the diseased patients, (108 of 119); defects were generally located within the territory of the appropriate artery, given the considerable overlap between RCA and LCx zones. Nonspecific defects in the diseased groups were rare (3 of 119); thus 105 patients in the diseased groups were classified as abnormal and 14 as normal; 9 of these 14 patients were interpreted as normal and 5 as borderline or showing mild disease according to visual analysis. The average quantification results for all groups studied are presented in Table 2. The RCA defects in men were smaller than defects in other territories, mainly due to attenuation artifacts. Higher severity products generally corresponded to larger defects.

To assess the effect of possible misalignment on the region-growing procedure, we visually examined the quality of fit and region-growing results in all patients. We observed small discrepancies of tilt (<4 deg) and sizing (<5%) in five patients with a large amount of external activity adjacent to the myocardium, which had not been removed by masking procedures. In three patients with severe defects in the LAD territory, a "ballooning" of the apex significantly modified the shape of the ventricle. The registration program correctly aligned such data, but a small part of the myocardial wall was positioned outside the template and region-growing outlined that area as a portion of the defect. In 10 other patients, the region-growing technique produced small defects due to shape differences between the registered patient data and the normal template; nevertheless, these defects were negligible in size (<2%) or located outside the expected defect territories. Such small differences in shape occurred sometimes at the edge of the myocardium. Presumably, the high variation values on the edges (Fig. 2) prevented the creation of spurious defects of a larger size.

We observed a significant overlap of territories between the RCA and LCx regions in men (Fig. 4), which caused an incorrect assignment of the perfusion zone in some patients (Table 1). The male LCx group contained two patients in whom the defect extended significantly toward the high lateral zone; in other patients (n = 10), it was located in the inferolateral and lateral regions. The average RCA defects were smaller than the LCx defects in men; therefore, in some RCA patients, most of the defect was actually located in the LCx zone (Tables 1, 2). In women, however, these territories were better separated (Tables 1, 2).

DISCUSSION

Maps of hypoperfusion zones were applied to assign myocardial perfusion lesions to particular coronary arteries. These maps can be used in combination with normal templates to detect and classify defects in a fully automated fashion. The region-growing technique classified defect voxels into contiguous regions which facilitated calculation of quantitative parameters. Furthermore, small isolated regions of abnormal voxels were not marked because the algorithm searched for only a limited number of defects. Robust performance of the region-growing algorithm, as reflected in Table 1, could be attributed to the incorporation of the three-dimensional variation map and accurate alignment of the test images. The application of the region-growing technique will have to be further evaluated in the detection and localization of multivessel disease. Furthermore, the effect of myocardial wall thickness on region-growing quantification will have to be assessed (*7*). Automated voxel grouping during the region-growing procedure distinguishes our technique from the bull's-eye approach (*8,9*). In the bull's-eye method, pixels on the polar map are tested against normal criteria and subsequently a clustering algorithm is applied to eliminate isolated abnormal pixels.

The natural, visual representation of quantification results in our approach simplifies image interpretation. If there are position, alignment or shape differences between the patient data and reference model, these discrepancies are immediately evident and directly compared with the original data because both the actual patient data and the defect are visible (Fig. 3). Integrated images of tomographic slices and outlined defects can be displayed using existing conventional display formats. Therefore, the inter-

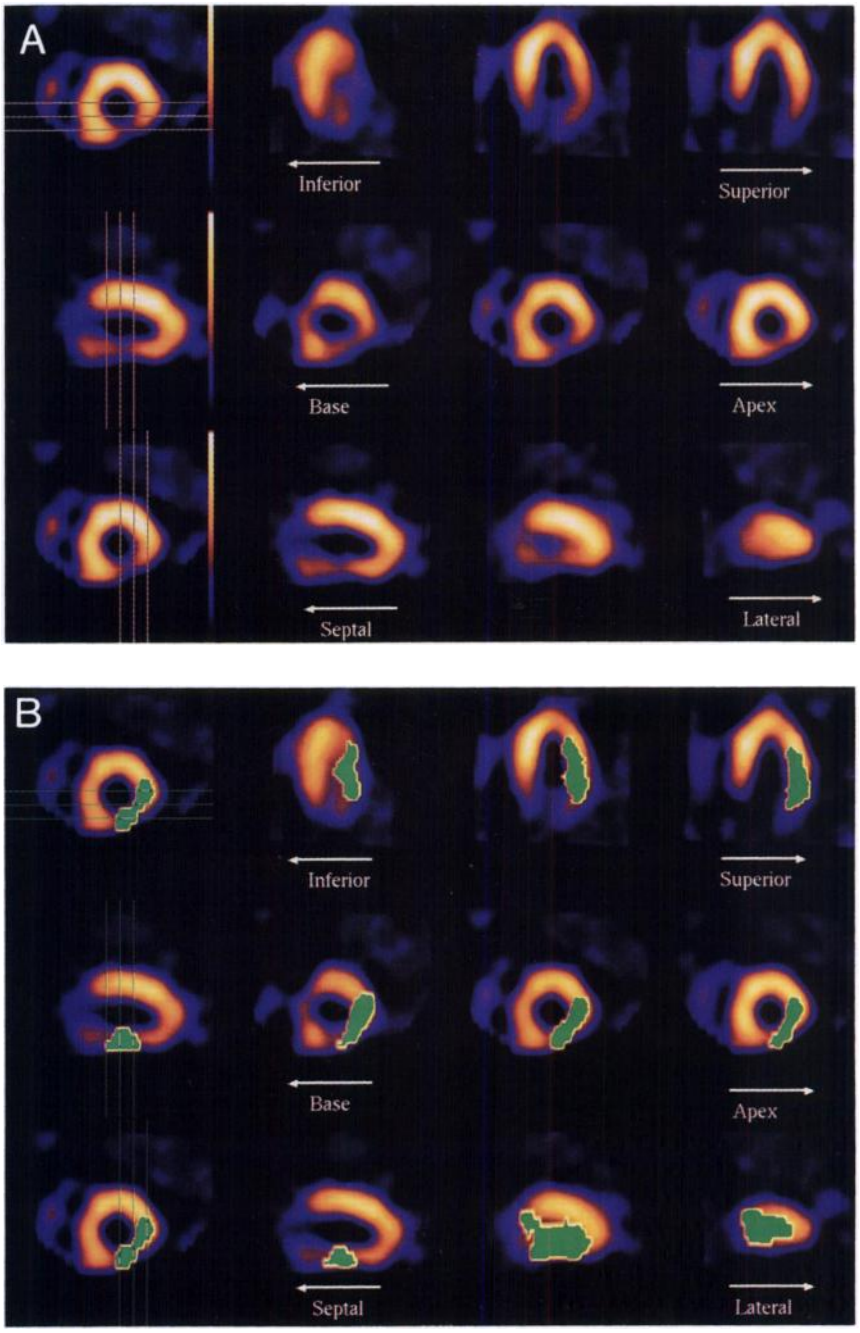

FIGURE 3. Small LCx defect in a test patient (A) and results of the region-growing procedure (B). The region below 2 s.d.s is marked as green. Quantification results are: number of voxels (455), absolute volume (30 cm^3), relative defect size (11%); defect severity (3.2); severity product (29); percentage of defect contained in territories: LAD (0%), RCA (26%), LCx (89%), undesignated (9%).

pretation of quantitative results in cases of borderline scans or when motion and attenuation artifacts are present may be more straightforward. It has been shown that errors in specifying sizing and alignment parameters can produce artifacts on the polar map display (*10,11*). These errors may produce inaccuracies in quantification and localization of defects; thus the analysis of the original images is always recommended (*10,11*). Although several approaches have been previously developed to visualize maximal-count profiles in three dimensions (*12,13*), these techniques plot the values of the circumferential/radial profiles derived from the short-axis slices on the three-dimensional surface. Such visualization can camouflage positional or distortion errors in the same manner as the two-dimensional polar map.

Fully automated fitting of patients to the reference templates in our approach eliminated potential operator subjectivity and reduced alignment errors as compared to manual methods. Although the bull's-eye method has been shown to be highly reproducible when combined with subjective visual interpretation of scans (*14*), the adjustment of orientation parameters and image interpretation may require experienced readers to ensure good reproducibility. The fitting errors of the registration procedure were assessed earlier quantitatively (*1*). In this study, small visual discrepancies in five severely abnormal patients were found. These observations were based on subjective image interpretation, which cannot be used as the absolute standard. Visual assessment of registration errors varied signif-

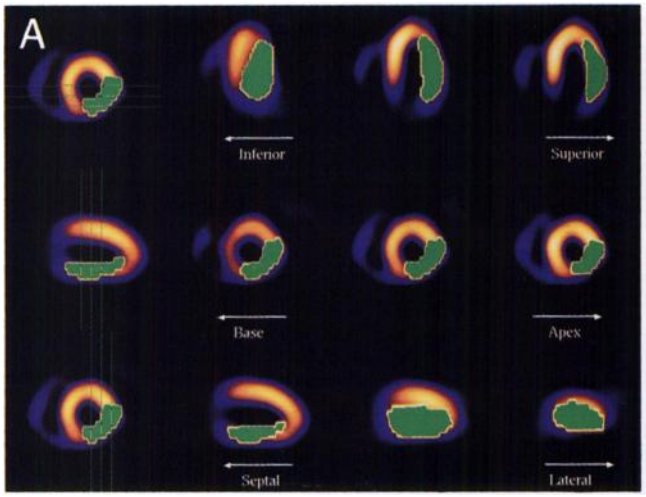

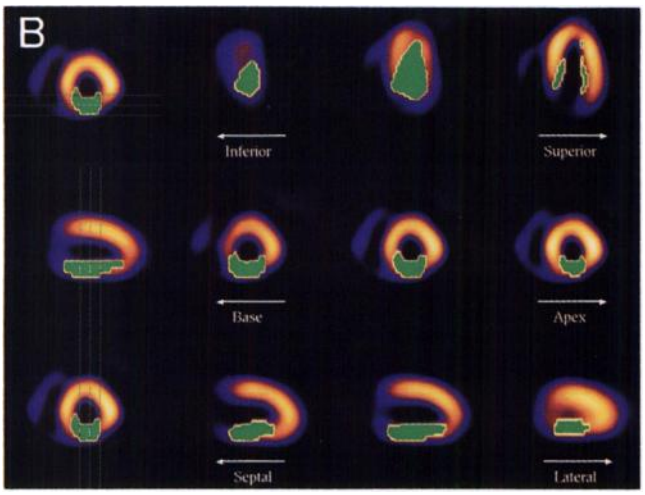

FIGURE 4. Average LCx (A) and RCA (B) territories (green) overlaid on their respective disease templates. The territories were derived by region-growing on the disease templates. LCx template included 14 patients; the RCA template 28 patients.

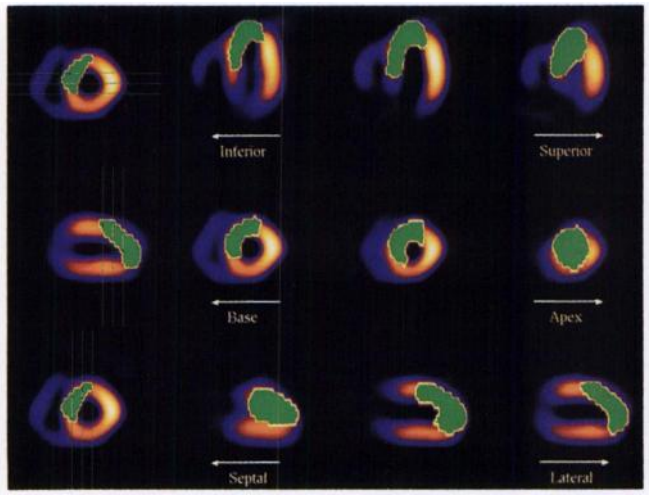

FIGURE 5. Average PLAD territory (green) overlaid on the PLAD disease template accumulated from 26 patients.

icantly, depending on viewing parameters such as orientation, color table and display threshold.

Other investigators have previously applied the bull's eye quantification scheme (*8*) to characterize the territories of the three major coronary arteries (*15,16*). The LAD, RCA and LCx territories were reported in the polar map format; on this display, these three territories were represented as nonoverlapping geometric areas. In our study, we found a significant overlap between the LCx and RCA perfusion territories in our male group. Our approach, however, differed in several aspects:

1. Technetium-99m-sestamibi scans were analyzed.
2. Automated data registration was used.
3. The defect maps were created on three-dimensional templates.
4. Somewhat different angiographic criteria were assigned.

Specifically, no overlap of the LCx and RCA territories in previous studies (*15,16*) could have been the result of the different angiographic criteria for dividing the patients into these two groups. For example, some LCx patients were assigned to the RCA group based on the dominance of the arterial system, which is usually not known a priori. The overlap between the RCA and LCx territories was also reported by Segal et al. (*17*).

At this stage, we did not attempt to optimize the criteria for detecting defects or assigning perfusion zones. Moreover, rest studies were not quantified at this time; the comparison between the regional defect quantification of stress and rest images will be necessary to provide an estimate of ischemia. Because the goal of our study was to determine perfusion territories, the patient population was limited to those with single-vessel disease and well-defined defects according to strict angiographic criteria. For example, patients with stenoses between 50% and 70% were excluded to obtain a better definition of the composite

TABLE 1
Patients with Defects in Designated Territories

Stenosis site	No. of patients	Defect size (≥2%)	Defect assigned to the territory			
			LAD	RCA	LCx	Unassigned
Women						
None	20	4	1	0	0	3
LAD†	12	11	11	0	0	0
RCA	8	8	0	8	0	0
LCx	7	5	0	1	3	1
Men						
None	29	5	0	0	2	3
PLAD	26	24	23	0	0	1
DLAD	24	23	22	0	0	1
RCA	28	24	2	15	7	0
LCx	14	13	0	3	10	0

*Defect size greater than 2% of the myocardial volume.
†For women, the patients with proximal and distal LAD stenoses were combined into one category.

TABLE 2
Average Defect Parameters

Stenosis site	Defect size (%)	Severity product†	% Defect*			
			LAD	RCA	LCx	Unmarked region‡
Women						
None	1 ± 3	3 ± 7	—	—	—	—
LAD	21 ± 15	78 ± 65	65	21	6	23
RCA	22 ± 13	78 ± 47	13	72	16	15
LCx	16 ± 16	58 ± 56	6	19	38	34
Men						
None	2 ± 5	4 ± 12	—	—	—	—
PLAD	26 ± 15	104 ± 74	71	2	3	22
DLAD	23 ± 14	90 ± 60	65	7	8	21
RCA	13 ± 11	37 ± 38	18	47	38	17
LCx	23 ± 16	91 ± 67	8	36	55	21

*Percentage of defect contained in a given territory. Due to territory overlap, the sum of the percentage contained in all territories can be higher than 100%.

†Average number of s.d.s below the mean in the defect region multiplied by the defect relative size (in % of myocardium).

‡Average percentage of the defect positioned outside all designated territories.

perfusion zones. Clinical validation of the technique would include patients with multivessel disease, rest studies and broader angiographic criteria. In a preliminary work, we have found that defects representing the full clinical spectrum can be properly characterized by our method (*18*).

CONCLUSION

By fitting homogenous groups of diseased patients to normal reference templates, perfusion territories corresponding to the major coronary arteries could be demarcated. An automated method was used to discern, outline and quantify defects in patients with well-characterized, single-vessel disease. In test patients, the method provided an appealing, natural display of defect extent and severity. The measure of the defect overlap with demarcated perfusion territories provided criteria for automated assignment of defects to specific coronary arteries. These techniques may allow fully automated and standardized interpretation of myocardial tomography.

ACKNOWLEDGMENTS

The authors thank Dr. Frank Prato for useful discussions and Ms. Soraya Ali for help in preparing the manuscript.

REFERENCES

1. Slomka PJ, Hurwitz G, Stephenson JA, Cradduck TD. Automated alignment and sizing of myocardial stress and rest scans to three-dimensional normal templates using an image registration algorithm: a method for reproducible quantification. *J Nucl Med* 1995;36:1115–1122.
2. Hurwitz GA, MacDonald AC. Stenoses of the left anterior descending artery: predominant role in stress-induced pulmonary uptake of thallium-201. *Can J Cardiol* 1994;10:982–988.
3. Hurwitz GA, Saddy S, O'Donoghue JP, Ali SA, et al. The VEX-test (vasodilator plus exercise) for myocardial scintigraphy with T1-201 and sestamibi: effect on abdominal background activity. *J Nucl Med* 1995;36:914–920.
4. Faber TL, Stokely EM. Orientation of 3-D structures in medical images. *IEEE Trans Pattern Anal Machine Intell* 1988;10:376–380.
5. Press WH, Teukolsky SA, Vetterling WT, Flannery BP. *Numerical recipes in C*, 2nd edition. New York NY: Cambridge University Press; 1992:408–412.
6. Gonzales RC, Woods RE. *Digital image processing*. Reading MA: Addison-Wesley Publishing Co.; 1992:298.
7. Galt JR, Garcia EV, Robins WL. Effects of myocardial wall thickness on SPECT quantification. *IEEE Trans Med Imag* 1990;9:144–150.
8. Garcia E, Van Train K, Maddahi J, et al. Quantification of rotational thallium-201 myocardial tomography. *J Nucl Med* 1985;26:17–26.
9. Garcia E, Cooke CD, Van Train KF, et al. Technical aspects of myocardial SPECT imaging with technetium-99m sestamibi. *Am J Cardiol* 1990;66:23E–31E.
10. De Puey EG, Garcia EV. Optimal specificity of thallium-201 SPECT through recognition of imaging artifacts. *J Nucl Med* 1989;30:441–449.
11. De Puey EG. How to detect and avoid myocardial perfusion SPECT artifacts. *J Nucl Med* 1994;35:699–702.
12. Cooke CD, Garcia EV, Folks RD, Peifer JW. Three-dimensional visualization of cardiac single photon emission computed tomography studies. In: Robb RA, ed., *Visualization in biomedical computing. SPIE* 1992;1808:671–675.
13. Loboguerro A, Perault C, Gibold J, et al. Shape preserving three-dimensional display of myocardial scintigraphic data. *Nucl Med Commun* 1994;15:417–421.
14. Alazraki NP, Krawczynska EG, DePuey EG, et al. Reproducibility of thallium-201 exercise SPECT studies. *J Nucl Med* 1994;35:1237–1244.
15. DePasquale EE, Nody AC. De Puey E, et al. Quantitative rotational T1-201 tomography for identifying and localizing coronary artery disease. *Circulation* 1988;77:316–327.
16. Maddahi J, Van Train KF, Prigent F, et al. Quantitative single photon emission computerized thallium-201 tomography for the evaluation of the coronary artery disease: optimization and prospective validation of a new technique. *J Am Coll Cardiol* 1989;14:1689–1699.
17. Segal GM, Atwood JE, Botvinick EH. Variability of normal coronary anatomy: implications for the interpretation of thallium-SPECT myocardial perfusion images in single-vessel disease. *J Nucl Med* 1995;36:944–951.
18. Slomka PJ, Hurwitz GA, Murray K, Stephenson JA. Clinical validation of the automated fitting method for fitting and comparing myocardial SPECT images to three-dimensional reference templates [Abstract]. *Clin Nucl Med* 1995:20;36:944–951.